Journal of the Taiwan Institute of Chemical Engineers 79 (2017) 23–30

Contents lists available at ScienceDirect

Journal of the Taiwan Institute of Chemical Engineers

journal homepage: www.elsevier.com/locate/jtice

Biodiesel production by pervaporation-assisted esterification and pre-esterification using graphene oxide/chitosan composite membranes

Yu-Kai Lin[a], Van-Huy Nguyen[b], Joseph Che-Chin Yu[a], Ching-Wei Lee[a], Yu-Heng Deng[a], Jeffrey C.S. Wu[a,*], Kevin C.W. Wu[a], Kuo-Lun Tung[a], Cheng-Liang Chen[a]

[a] Department of Chemical Engineering, National Taiwan University, Taipei 10617, Taiwan
[b] Faculty of Chemical and Environmental Engineering, Lac Hong University, No. 10 Huynh Van Nghe, Buu Long, Bien Hoa, Dong Nai, Vietnam

ARTICLE INFO

Article history:
Received 15 November 2016
Revised 10 June 2017
Accepted 13 June 2017
Available online 18 July 2017

Keywords:
Pervaporation (PV)
Esterification
Pre-esterification
Graphene oxide/chitosan (GO/CS)
Composite membrane
Biodiesel production

ABSTRACT

In this study, a series of novel graphene oxide/chitosan (GO/CS) composite membranes was successfully synthesized and fully characterized. The performance of GO/CS composite membrane was then evaluated by integrating with the esterification of acetic acid with ethanol or the pre-esterification of palmitic acid with methanol, both essential in biodiesel production. Typically, esterification and pre-esterification are reversible reactions, which are limited by chemical equilibrium, resulting in a low product yield. In our study, reaction and separation were conducted in two separated steps or in a single one by means of a catalytic membrane. The preferential removal of water through the membrane in a PV-assisted process enhanced the conversion. The results show clearly that temperature, wt% of embedded GO within a polymeric CS-based membrane, and initial ratio of alcohol/acid are important parameters to enhance conversion because it acts on the kinetics of both pervaporation and esterification/pre-esterification. The enhanced catalytic membrane of the PV-assisted pre-esterification can only be observed when a proper amount of Amberlyst-15 catalyst is used. Additionally, the results of PV-assisted esterification/pre-esterification show that the ratio of water removal (by membrane) and water production (by esterification) rates play a significant role in evaluating the catalytic membrane. Under specific conditions, the conversions of PV-assisted esterification and pre-esterification by the catalytic membrane could be higher than those without PV-assisted up to 8% and 20%, respectively. This process could offer a key technology for biodiesel production in the future.

1. Introduction

To date, pervaporation (PV) is the core and key point of current membrane research. PV could effectively shift its equilibrium position toward higher conversion by selectively removing one or more product species from the reaction mixture [1,2]. It has found practical applications for PV that could be classified under three categories: (a) dehydration with solvents, (b) separation of anhydrous organic mixtures, and (c) removal of water from aqueous solutions [3]. Among their applications, a hybrid PV-assisted esterification process that applied to the production of eco-friendly biodiesel is an effective and a potential method for producing esters [4–6]. This technique, in the corresponding experiment without membrane-assistance, is possible to shift the equilibrium toward higher conversion by selectively removing the water produced. To have a better potential for biodiesel production at reasonable costs, much interest has been taken in using low-quality plant oil as the cost advantageous feedstock. However, the low-quality plant oil has a significant amount of free fatty acids (FFA, 2–7 wt% in the feedstock) which might cause several serious concerns, such as a slow-down of the base-catalyzed transesterification, loss of the produced biodiesel [7]. Therefore, the pre-esterification is often considered before the transesterification to reduce the amount of FFA by esterifying FFA into their methyl esters preliminarily (target of 0.5 wt% FFA). In this work, it would be quite valuable to explore the biodiesel production by both PV-assisted esterification and pre-esterification.

In PV process, the non-toxic and biodegradable polysaccharide polymer, chitosan (CS), is extensively applied across a material membrane. Several advantages have been offered by CS-based polymers such as naturally abundant, appreciable hydrophilic, high chemical stability, excellent forming ability, and facile filming

* Corresponding author.
E-mail address: cswu@ntu.edu.tw (J.C.S. Wu).

http://dx.doi.org/10.1016/j.jtice.2017.06.031
1876-1070/

process [8,9]. However, polymer-based membranes, in general, still face a lot of concerns, such as weak mechanical strengths and easy swelling after the long-term operation, resulting in reducing the separation performance [10]. A promising strategy for improving the physical properties of CS-based membranes is embedding inorganic nanoparticles within a polymeric phase, such as silica [11], calcium aluminosilicate [12], titanium dioxide [13], iron oxides [14–16], silver [17], and graphene oxide [18–21]. Among inorganic fillers, graphene oxide (GO) has attracted intensive attention. It contains various groups of oxygen functional, *e.g.*, hydroxyl, epoxide, diol, ketone, and carboxyl, which chemically react to the amine group of CS to form a bond between GO and biopolymer (CS) [20,21]. It is important that GO also exhibits remarkable mechanical strength, relatively large surface area, and low costs [22]. In this study, a novel modified graphene oxide/chitosan-based (GO/CS) composite membrane is developed. We expect that GO/CS membrane could give advantages of both organic–inorganic membranes, such as high chemical and thermal stability, outstanding mechanical properties, and free of swelling.

In summary, to develop membranes with the desired physicochemical properties and long-term stability, a different amount of GO within a polymeric CS-based membrane was successfully embedded and analyzed by FTA-32 goniometer, FE-SEM, TGA, FT-IR. Amberlyst 15, among the best commercial heterogeneous acid catalysts with distinct advantages including inexpensive, high physicochemical stable, environmentally benign, nontoxic [23], and easily recyclable [24]. It is used to evaluate the efficiency of GO/CS composite membranes in catalytic esterification of acetic acid (AcOH) with ethanol (EtOH) and pre-esterification of palmitic acid (PamOH) with methanol (MeOH) reactions. Additionally, the optimization of the experimental conditions, including temperature, the amount of Amberlyst-15 catalyst and initial ratio of alcohol/acid, is also explored. To the best of our knowledge, such a diverse study that evaluates different wt% of GO within a polymeric CS-based membrane in PV-assisted esterification and pre-esterification for biodiesel production has not been reported before.

2. Experimental

2.1. Preparation of graphene oxide/chitosan (GO/CS) composite membrane

A series of graphene oxide/chitosan (GO/CS) composite membranes (1, 2, 3, and 4 wt% GO embedded CS) was prepared by using a doctor-blade method. Firstly, chitosan powders (Sigma-Aldrich, 200–800 cps) were dissolved in deionized water with 2 wt% acetic acid (J.T. Baker, >99.7%). To remove the impurities, the solution was subsequently filtered by the paper of a pore size of 6 μm. Then, a given amount of GO (E WAY Technology Co., LTD, China) was added into the as-prepared CS solution and stirred vigorously for 3 h. Next, a 1:33 dilution of cross-linking glutaraldehyde (GA) solution was prepared by dissolving glutaraldehyde (Sigma-Aldrich, 50 wt% in H_2O) in deionized water with 1 wt% H_2SO_4 (Sigma-Aldrich, 95–99%). As follows, the formed casting solution was reacted with a certain amount of 2.5 wt% GA dilution solution for 30 min. Afterward, the casting solution was carefully poured over the glass plate, then it was cast to form a membrane with a thickness of several micrometers. As follows, the membrane was slowly dried at 50 °C for 8 h, then peeled from the glass plate. Finally, the membrane is trimmed to fit the size of the PV module (39 mm circular diameter). For comparison, the pristine CS composite membrane was also prepared by the similar method.

2.2. Characterization of membranes

The contact angle between water and membrane surface is widely used to understand the hydrophilic property of membrane. Herein, the water contact angle was measured by the sessile drop method using an FTA-32 goniometer (First Ten Angstroms, USA). The fracture surface morphology on top and cross-section views of membranes were observed by Field Emission Scanning Electron Microscopy (FE-SEM). The composition and changes in thermal stability of the membranes were determined by the Thermogravimetric analyzer (TGA, Pyris 1 TGA, Perkin-Elmer, USA) at a heating rate of 10 °C/min up to a final temperature of 600 °C under the inert nitrogen flow rate of 20 ml/min. Chemical functional groups of membranes were analyzed using a Fourier transform infrared spectroscopy (FT-IR, Nexus 670 spectrometer, Thermo Nicolet, USA).

2.3. Experimental apparatus

The experiments of PV-assisted esterification were performed in the combination of a three-neck round-bottom flask reactor and a membrane module, as shown in Scheme 1. The flask reactor (130 ml) was equipped with a reflux condenser and thermocouple in a temperature-controlled oil bath. The initial reaction mixture of EtOH: AcOH (1:1, 2:1, and 3:1 in mol/mol) was heated to the desired reaction temperature (50–70 °C). The reaction was started by adding a desired wt% of Amberlyst 15 solid catalyst (1.50–2.25 wt%) to the flask reactor. The vacuum was the drive-force used for permeation while the retentate was circulated by a peristaltic pump. The membrane module (PV module) was made of 316 stainless steel and the composite membrane with an effective membrane area 706.9 mm^2 (39 mm circular diameter). The PV temperature was maintained at the same value of esterification temperature by an electric heating coil wound around the PV module.

For the PV-assisted pre-esterification, the initial reaction mixture of MeOH: PamOH (20:1 in mol/mol) was heated to the desired reaction temperature (50–60 °C). The reaction was started by adding a desired wt% of Amberlyst 15 solid catalyst (5–10 wt%) to the flask reactor. 4 wt% GO/CS composite membrane was used to evaluate the performance. The PV temperature was maintained at the same value of pre-esterification temperature.

During the PV-assisted reactions, the product samples were taken from the three-necked flask and analyzed every 2 h. The product and reactant compositions were determined by using a Hewlett Packard gas chromatograph (HP 6890) equipped with an HP-INNOWAX capillary column (0.32 mm in ID and 30 m in length) and flame ionization detector. It notes that the amount of acetic acid, which was removed by a membrane, was negligible. The conversion and flux were defined as follows.

$$\text{Conversion } (\%) = \left(1 - \frac{\text{detected acid}}{\text{initial acid}}\right) \times 100\% \quad (1)$$

$$\text{Total flux } (\%) = \frac{\text{Permeate weight}}{\text{Membrane area } \times \text{ Time}} \quad (2)$$

$$\text{Partial flux of } i = \text{Total flux} \times \text{wt\% of } i \quad (3)$$

3. Results and discussion

3.1. Characterization of GO/CS composite membrane

The contact angles of all the different wt% of graphene oxide in the membrane were measured to evaluate the hydrophilicity of membranes. Fig. 1 clearly shows that 2 wt% of GO has the smallest contact angle (66.4°) among the membranes, suggesting that

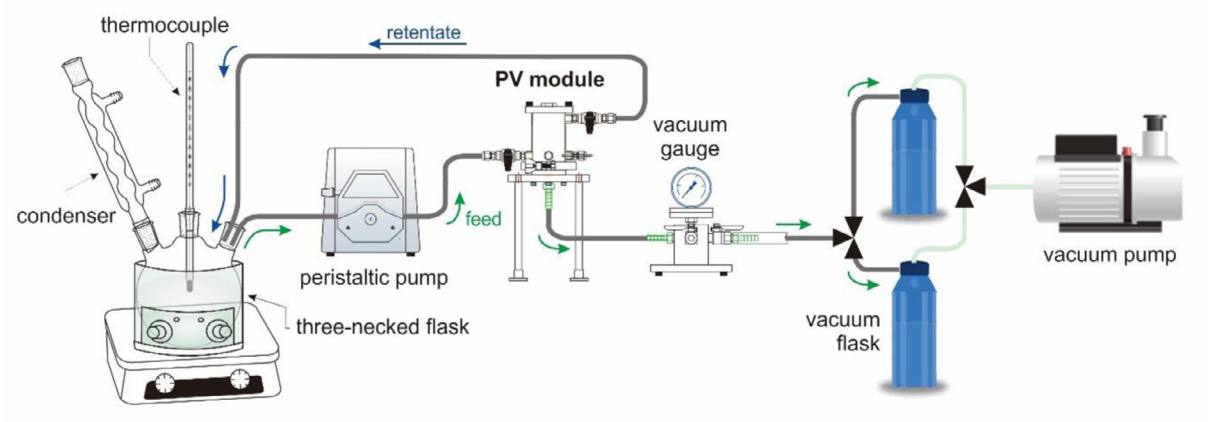

Scheme 1. The scheme diagram of pervaporation-assisted reaction using graphene oxide/chitosan composite membranes.

Table 1
Assignments of IR bands to vibrational modes of atomic groups.

Group	Vibrational mode	Assigned wavenumber (cm^{-1})
–C–O–C– in glycosidic linkage	C–O stretching band	1085
	C–H scissoring bending	1151
C–O	N/A	1257
$–CH_2–$ in pyranose ring	C–H symmetrical or asymmetrical stretching	1320
$–CH_3$ in amide	N/A	1380
O–H, C–H in the ring	N/A	1415
Amide	–NH– bending	1560
Amide (amide I band)	C=O scissoring bending	1651

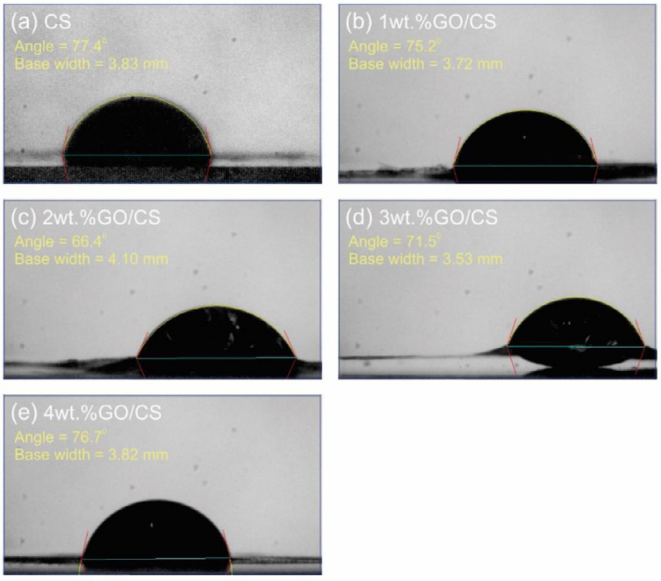

Fig. 1. Contact angle at different wt% of graphene oxide in composite membranes: (a) CS, (b) 1 wt% GO/CS, (c) 2 wt% GO/CS, (d) 3 wt% GO/CS, and (e) 4 wt% GO/CS.

it has the most hydrophilic property [25]. The contact angle difference is insignificant between the pristine CS and 1 wt% GO embedded CS (77.4° and 75.2°, respectively) while 2 wt% GO embedded CS shows the lowest contact angle. The value of contact angles gradually rises up when increasing the embedding amounts to 3–4 wt% (in the range of 71.5°–76.7°). It notes that there are a lot of hydrophilic functional groups in GO, such as epoxide, carbonyl, and carboxyl groups [26–28]. Therefore, increasing the embedding amounts would theoretically drop the contact angle. However, the experimental result shows that the contact angles would gradually increase when embedding amounts are extended to 3–4 wt%. Increasing embedding amounts would affect the dispersion ability of GO, resulting in observation of a gradual increase in contact angle.

The FE-SEM was conducted to explore the morphologies and interfacial interactions of different membranes. Fig. 2 (a–d) shows the images of surfaces from the top view of layers. The surfaces of membranes clearly display a smooth morphology. It reveals that the membrane surface becomes partially rougher as the embedding amounts of GO are increased. The surface of membranes possesses homogeneity highly, suggesting that both of GO and CS are miscible. However, it has some small dots extruded from the surface in 3 wt% GO/CS composite membrane, which might be attributed to the aggregation of GO particles. This result is consistent with the notion that embedding amounts would affect the dispersion ability of GO, resulting in changing the contact angle. The fractography of the surface from the cross-sectional view of the membrane are shown in Fig. 2 (e–h), revealing that the layer thickness is in the range of 4–7 μm. Additionally, this result could provide a direct information regarding the physical cross-linking and chain entangling of the chitosan. The cross-sections of the membranes show that the density of the inner structure of GO/CS layers increases apparently, in comparison with these of pristine CS membrane. This result indicates the strong interaction between GO and CS. The thickness of CS layer is 6.67 µm, while those of GO/CS membrane is in the range of 3.67–6.38 µm. The observed result is similar to a previous report in the literature [21].

FT-IR was conducted to reveal the interaction between GO and CS by using different embedding amounts on GO and the possible changes in the structure during the reaction. In Fig. 3(A), the dominant peaks are observed at 1085, 1151, 1257, 1320, 1380, 1415, 1560, 1651 cm^{-1}, which have already been described in previous studies [29,30]. The bands at 1085 and 1151 cm^{-1} are attributed to

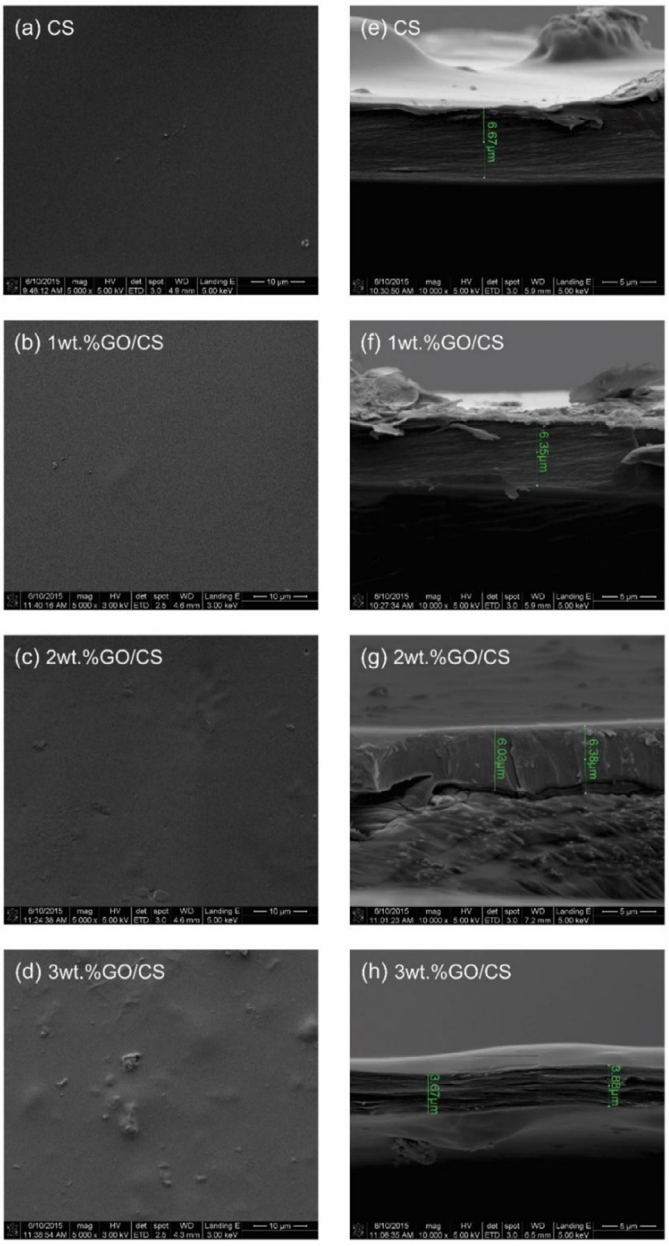

Fig. 2. FE-SEM micrographs of surfaces from the top view and the cross-sections view of composite membranes: (a, e) CS, (b, f) 1 wt% GO/CS, (c, g) 2 wt% GO/CS, (d, h) 3 wt% GO/CS.

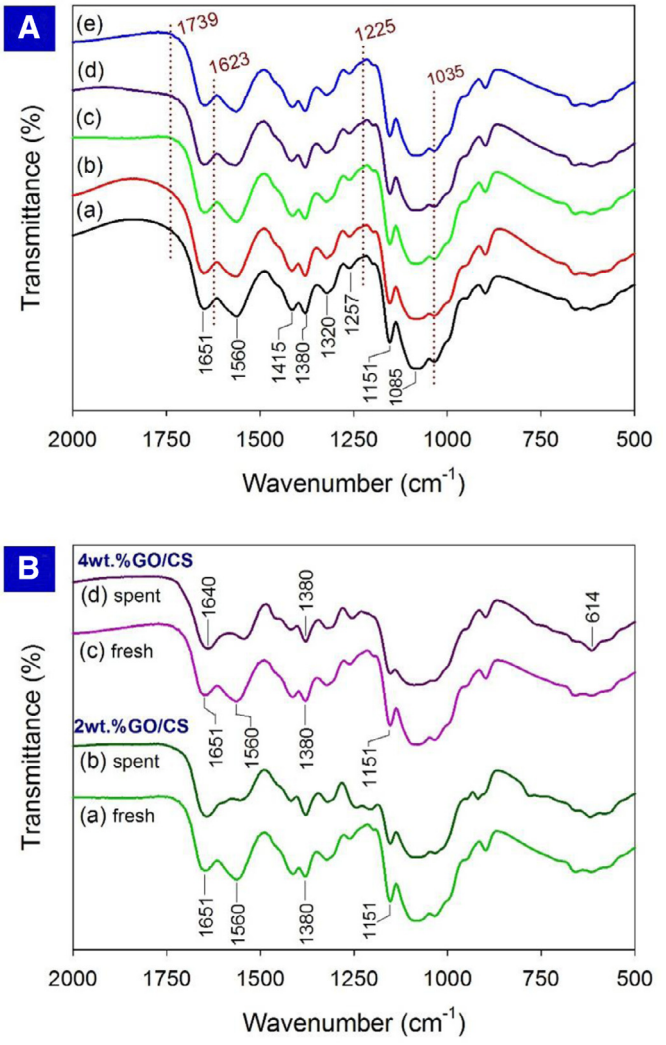

Fig. 3. FT-IR spectra of the composite membranes: (A) different wt% of GO in membranes (a) CS, (b) 1 wt% GO/CS, (c) 2 wt% GO/CS, (d) 3 wt% GO/CS, and (e) 4 wt% GO/CS; (B) the fresh and spent of membrane (a) 2 wt% GO/CS (spent), (b) 2 wt% GO/CS (fresh), (c) 4 wt% GO/CS (spent) and (d) 4 wt% GO/CS (fresh).

(–C–O–C–) group in glycosidic linkage. The band at 1257 cm^{-1} is ascribed to the (C–O) group. The band at 1320 cm^{-1} corresponds to a ($–CH_2–$) group in pyranose ring. The band at 1380 cm^{-1} is attributed to ($–CH_3$) group in amide group. The peak at 1415 cm^{-1} corresponds to vibrations of (O–H) and (C–H) groups in the ring. The peaks at 1560 and 1651 cm^{-1} are assigned to (–NH–) and (C=O) groups, respectively, in an amide. It is worth noting that embedding GO on CS composite membrane is almost identical to the pristine CS membrane due to the low embedding amounts (1–4 wt%). We did not emerge any characteristic bands of GO, such as the peaks located at 1035 cm^{-1}, 1225 cm^{-1}, 1623 cm^{-1}, and 1739 cm^{-1} [31,32]. It is possible that the structure of membrane might be changed during the reaction. Therefore, the fresh and spent samples are compared and shown in Fig. 3(B). For 2 wt% GO/CS membrane, changes at 1560 and 1151 cm^{-1} might be corresponded to the deforming of (–NH–) and (–C–O–C–) groups, respectively, during the reaction. Additionally, an increase of band located at 1651 and 1380 cm^{-1} corresponding to a region of the amide group is also recorded. Similarly, the changes of bands are also observed clearly for 4 wt% GO/CS membrane, suggesting that the esterification reaction might modify their structures. Table 1 summarizes the assignments of IR bands to vibrational modes of considered atomic groups in the present work.

The composition and changes in thermal stability of the different weight percent of GO membranes were fully tested by TGA. Firstly, the samples were heated to 110 °C for 10 min to remove the absorbed water totally. Then the TGA is recorded from 110 °C to 600 °C at a heating rate of 10 °C/min. As shown in Fig. 4, the trends of TGA are very similar with the main weight loss starting at about 250 °C for all the samples. This major loss of mass might correspond to glucopyranose ring of chitosan due to accounting for more than 95% of chitosan composition in every sample [33]. GO/CS composite membranes are thermally more stable than CS, as demonstrated in the previous study [34]. However, 4% GO/CS had more weight loss than 1% and 2% GO/CS composite membranes. This result could be inferred that even dispersion of GO particles might effectively change the thermal stability. As previously stated, the aggregation of GO particles might happen when over 3 wt% GO was embedded on the CS.

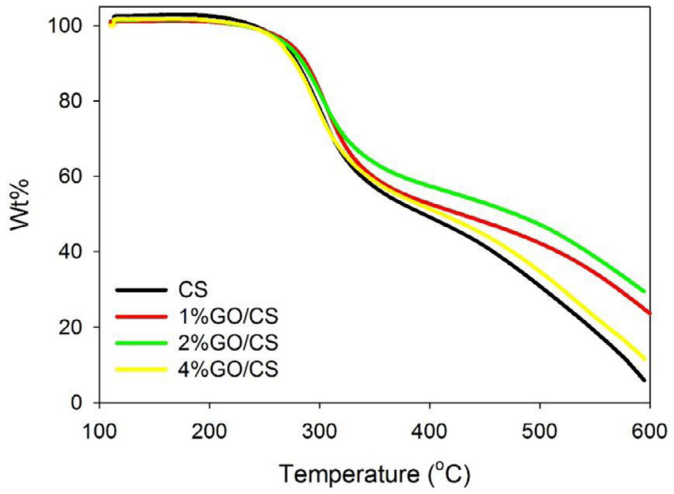

Fig. 4. TGA curve of different wt% of GO in composite membranes.

3.2. Pervaporation-assisted esterification in biodiesel production

3.2.1. The effect of reaction and pervaporation temperature

In this study, the reaction and pervaporation temperature are set below 75 °C, which is lower than that of the boiling point of ethanol (78 °C), to prevent the drastic evaporation and quick formation of vapor bubbles, resulting in reducing the catalyst ability. The esterification with or without PV-assisted under different temperature is thoroughly investigated and shown in Fig. 5. Obviously, the equilibrium conversion of PV-assisted esterification could be achieved higher than that of without using the PV module after 6–8 h in reaction. On the other hand, the result clearly reveals that the conversions (in the case without using the PV module) are increased when the temperature is elevated from 50 to 70 °C (as seen in Fig. 5(a)) at a fixed contact time under otherwise identical conditions. This results in a good agreement with our expectation that the esterification is an endothermic reaction. However, it is noted that the equilibrium conversions might be nearly equal (about 82% conversion) at the temperatures studied after 24 h. The enhancement of PV-assisted esterification is evident. An increase in temperature not only promotes the esterification but also accelerates the pervaporation. In other words, using PV-assisted at a high temperature is much more efficient than that at a low temperature. When the PV-assisted experiment is conducted at an elevated temperature, it will accelerate the permeation flux, resulting in increasing the rate of water removal (as seen in Fig. 5(c and d)). It notes that a decrease in water content in the reaction mixture will effectively enhance the esterification [35]. On the other hand, a molecular chain would be flexible at a high temperature. Therefore, the molecular is considerably much easy to pass through the membranes, resulting in raising a total flux. As our observation, the influences of temperature on esterification and pervaporation are not conflicted and on the same outlook.

In this study, we consider a coordination ratio (F) of rates that stands for the interaction between the water removal (by a membrane) and water production (by esterification). F is dimensionless that is found as a key factor to evaluate the performance of the PV-assisted esterification process. When the rate of water removal is larger than the water production rate ($F > 1$), the catalytic conversion has a potential to achieve 100%, but it is limited by the rate of water production (esterification). The comparison of the variations of F with time at different temperature (50 °C or 70 °C, respectively) is shown in Fig. 5(b). The ratio F increases with a rise in temperature. Initially, the rate of water removal is lower than that of the water production. During the reaction, it is gradually larger than that of production due to the effect of reactant consumption. Under investigated conditions, the coordination ratio (F) of rates could reach to 1.0 after 5–6 h in reaction. In other words, the PV-assisted esterification is limited by the esterification rate after 5–6 h in reaction, not pervaporation rate.

3.2.2. The effect of initial ratio of ethanol/acetic acid

The variations in the initial mole ratio of ethanol to acetic acid (EtOH/AcOH) have been carefully studied and carried out at a temperature of 70 °C, 3 wt% GO/CS composite membrane and 2.25 wt% of Amberlyst 15 catalyst. These results obtained are presented in Fig. 6. It clearly shows that the equilibrium conversion increases with the increasing of initial EtOH to AcOH (mol/mol). The equilibrium conversion of EtOH increased from about 64.4% at a feed mole ratio (alcohol to acid) of 1:1 to 84.6% at a feed mole ratio (alcohol to acid) of 3:1. It is to be noted that esterification of AcOH with EtOH is an equilibrium-limited chemical reaction. An excess of EtOH could lead to increased conversion due to the change of initial concentrations, which moves up the position of equilibrium. On the other hand, PV-assisted esterification still promotes the catalytic conversion under the different mole ratio of ethanol/acetic acid. Among the investigated conditions, the equilibrium conversion of EtOH could reach to 89.0% at a feed mole ratio (alcohol to acid) of 2:1.

3.2.3. The effect of amount of Amberlyst-15 catalyst

The esterification reaction was evaluated under the following conditions: $T = 70$ °C, EtOH/AcOH = 2:1, using 3 wt% GO/CS composite membrane. This experiment was conducted to understand the effect of the Amberlyst 15 catalyst (the proposed range of 1.50–2.25 wt%) loading to the reaction. As shown in Fig. 7, the higher amount of catalyst is employed, the better initial conversion could be achieved. As an amount of catalyst increases, it will provide more a total number of active sites available for the esterification. For 2.25 wt% Amberlyst 15 catalyst, the equilibrium conversion (about 85%) was reached within 6 h, whereas it took about 10 h to achieve that conversion for 1.50% catalyst loading. However, the reaction did not receive a significant improvement when raising the catalyst amount from 1.50 to 2.25 wt%. Although the initial reaction rate was faster at a higher amount of catalyst, all the experiments achieved a similar equilibrium conversion after 10 h of reaction.

3.2.4. Effect of GO embedding amounts on GO/CS composite membrane

Fig. 8 clearly reveals that it is impossible to observe a high initial conversion by using pervaporation-assisted esterification. After 5 h in reaction, the performance of 2–3 wt% GO/CS composite membranes could reach similar conversion that achieved by not-using the PV-assisted esterification. Even for 1 wt% GO/CS composite membrane, their performance is still lesser than that of none PV-assisted after 15 h in reaction. It is not a surprising result for PV-assisted esterification since the initial water removal rate is much lower than the water production rate. Therefore, it is initially limited by water removal rate, not the esterification rate. However, the removal rate is gradually increased while the production rate is moderately decreased during the reaction due to the fact of reactant consumption. In summary, for 2–3 wt% GO/CS composite membranes, PV-assisted esterification is limited by the esterification at the beginning of the reaction, and we could observe a high conversion performance after 5 h in reaction. For 1 wt% GO/CS composite membrane, the enhancement by PV-assisted would appear if the reaction time was prolonged.

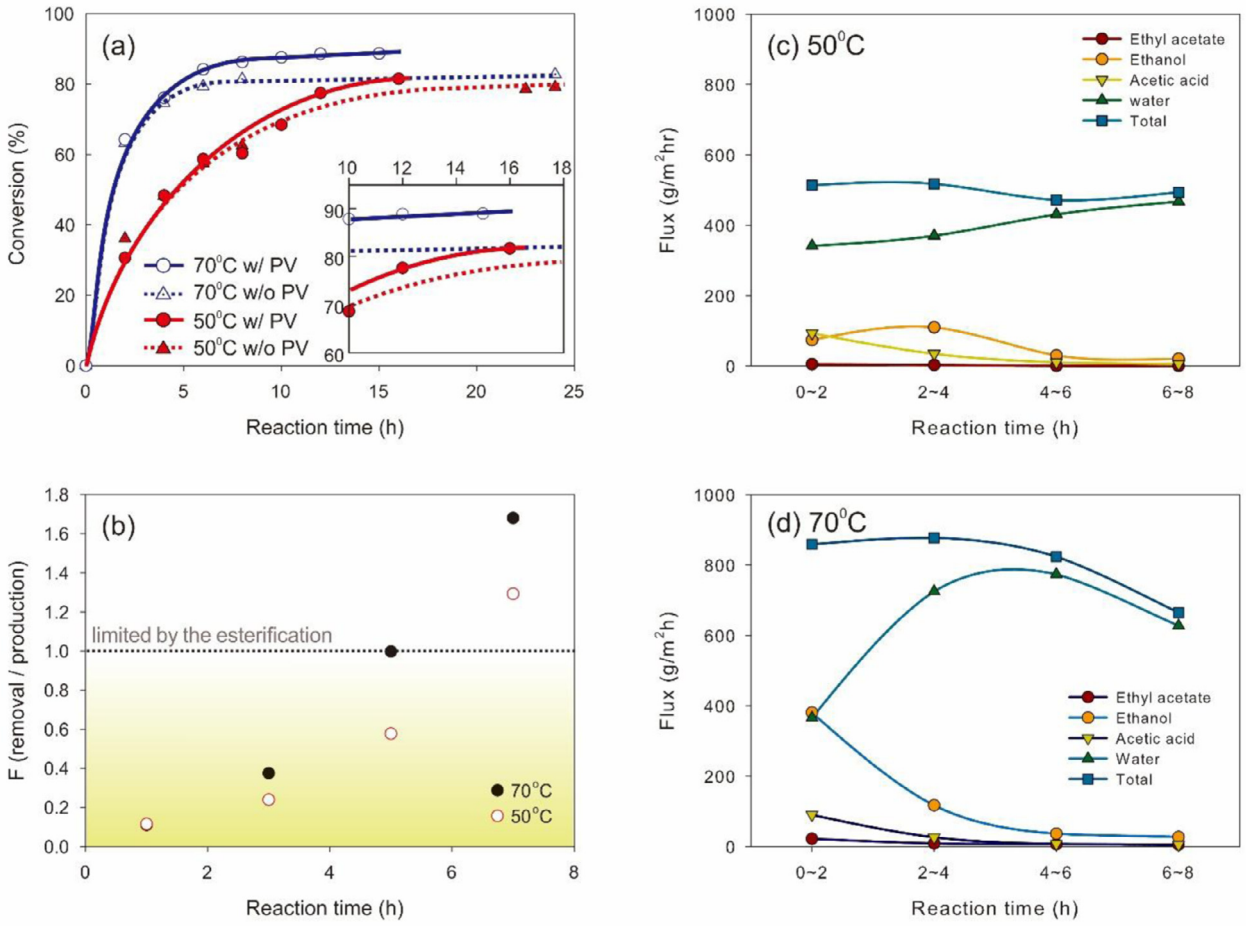

Fig. 5. The esterification of acetic acid with ethanol at different reaction temperature: (a) Conversion *versus* time, (b) comparison of the variations of F (water removal/water production), (c) permeation flux at 50 °C and (d) permeation flux at 70 °C. Operation conditions: $T = 50–70$ °C; initial ratio of EtOH:AcOH = 2:1; 2.25 wt% of Amberlyst-15 catalyst; 3 wt% GO/CS composite membrane. Lines are presented for guiding and are not based on a kinetic model.

3.3. Pervaporation-assisted pre-esterification in biodiesel production

3.3.1. The effect of PV-assisted, temperature of reaction and pervaporation

In the pre-esterification, methanol (MeOH) is used as the excess reagent in the reaction. The reaction and pervaporation temperature are set below 64.7 °C (the boiling point of methanol) to prevent the drastic evaporation. In this study, the pre-esterification with or without PV-assisted under 50 °C and 60 °C, respectively, is carefully investigated and shown in Fig. 9(a). Similar to the esterification of AcOH with EtOH process, the conversion of the pre-esterification of palmitic acid (PamOH) with MeOH is increased by the rise in temperature. A higher reaction temperature is more favored since pre-esterification is the endothermic reaction.

It is not possible to observe an improvement in the PV-assisted pre-esterification at a temperature of 60 °C, in comparison with non PV-assisted pre-esterification. The rate is limited by the pervaporation. In this case, the rate of water removal is much lower than that of the water production since a high temperature will significantly favor the rate of pre-esterification. The conversion for PV-assisted pre-esterification could be achieved a greater than that for none PV-assisted if the reaction time was prolonged.

To observe the limitation phenomenon by the pre-esterification, the temperature is designed at 50 °C. At the beginning of the reaction, the rate of the pre-esterification is still higher than that of pervaporation. However, a lower temperature would not significantly favor the rate of pre-esterification, in comparison with the reaction that is conducted at 60 °C. Therefore, as expected, we could observe an improvement on the PV-assisted pre-esterification after 2 h in reaction.

3.3.2. The effect of PV-assisted pre-esterification and amount of Amberlyst-15 catalyst

Fig. 9(b) indicates that there is no chance to observe an improvement in conversion by PV-assisted pre-esterification when using a high amount of Amberlyst-15 catalyst (10 wt%). The reason is that the water production is too much and over the capacity of pervaporation since a catalyst amount is significant. In other words, PV-assisted pre-esterification is limited by water removal rate (pervaporation step). By lowering to 5 wt% Amberlyst-15 catalyst, a decrease in catalytic conversion is observed. This phenomenon is assigned to the loss of active sites available for the reaction since the catalyst amount decreases. Additionally, a clear improvement trend on initial conversion is also noted between with and without PV-assisted. Under given conditions, PV-assisted pre-esterification is limited by the pre-esterification reaction. It expects that their conversion would be similar if the time was prolonged.

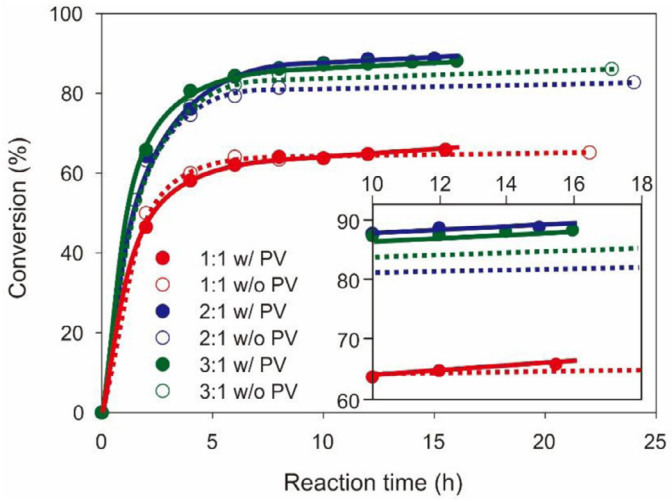

Fig. 6. Conversion *versus* time, esterification of acetic acid with ethanol at a different initial ratio of EtOH:AcOH = 1:1, 2:1, and 3:1 (mol/mol). Operation conditions: $T = 70\,^{\circ}C$; 3 wt% GO/CS composite membrane; 2.25 wt% of Amberlyst 15 catalyst. Lines are presented for guiding and are not based on a kinetic model.

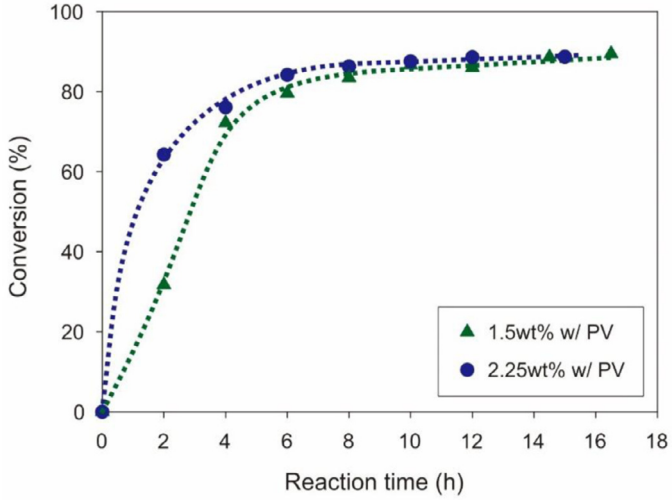

Fig. 7. Conversion *versus* time, esterification of acetic acid with ethanol at different amount of Amberlyst 15 catalyst (1.50 wt% and 2.25 wt%). Operation conditions: $T = 70\,^{\circ}C$, initial ratio of EtOH:AcOH = 2:1; 3 wt% GO/CS composite membrane. Lines are presented for guiding and are not based on a kinetic model.

4. Conclusions

In this study, a series of graphene oxide/chitosan (GO/CS) composite membrane was prepared and characterized by FTA-32 goniometer, FE-SEM, TGA, FT-IR. The performance of membrane was evaluated by integrating with the esterification of acetic acid with ethanol or the pre-esterification of palmitic acid with methanol, both essential in biodiesel production. The results clearly show that temperature, wt% of embedded GO within a polymeric CS-based membrane and initial ratio of alcohol/acid are important parameters to enhance conversion because it acts on both the kinetics of pervaporation and esterification/pre-esterification. Importantly, the enhanced catalytic membrane of the PV-assisted pre-esterification can only be observed when a proper amount of Amberlyst-15 catalyst is used. The catalytic membrane in PV-assisted esterification is promoted by 8% under the operating conditions at 70 °C, 2.25 wt% Amberlyst-15 catalyst and ethanol: acetic acid of 2:1. Regarding pre-esterification, the catalytic conversion in PV-assisted could be enhanced by 20% under the conditions at

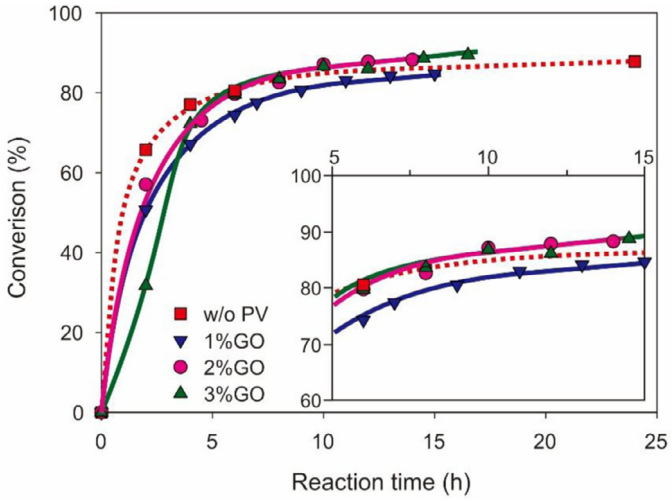

Fig. 8. Conversion *versus* time, non PV-assisted esterification and PV-assisted esterification of acetic acid with ethanol using 1–3 wt% GO/CS composite membranes. The operation conditions: $T = 70\,^{\circ}C$; initial ratio of EtOH:AcOH = 2:1; 1.50 wt% of Amberlyst 15 catalyst. Lines are presented for guiding and are not based on a kinetic model.

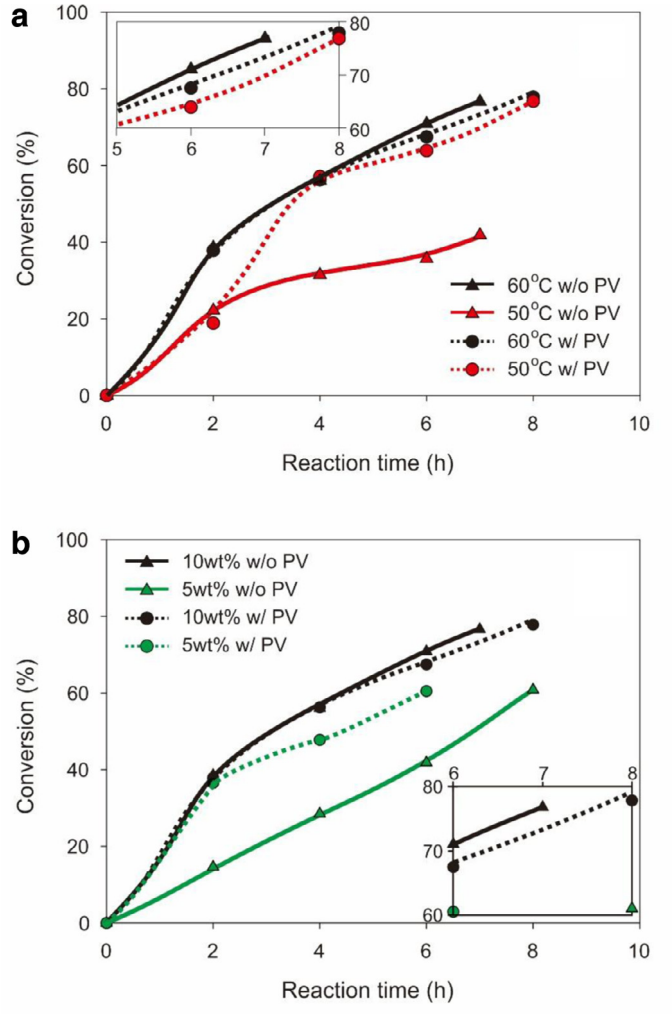

Fig. 9. Conversion *versus* time, non PV-assisted and PV-assisted pre-esterification of palmitic acid with methanol at different: (a) $T = 50$–$60\,^{\circ}C$ using 10 wt% of Amberlyst-15 catalyst, (b) 5–10 wt% of Amberlyst-15 catalyst at $T = 60\,^{\circ}C$. The operation conditions: Initial ratio of MeOH: PamOH = 20:1; 4 wt% GO/CS composite membrane. Lines are presented for guiding and are not based on a kinetic model.

50 °C, methanol: palmitic acid of 20:1, and 10 wt% Amberlyst-15 catalyst. Our study demonstrated that the ratio of water removal (by membrane) and water production (by esterification) rates plays a significant role in evaluating the catalytic membrane. This process could provide a key technology for biodiesel production in the future.

Acknowledgments

The authors gratefully acknowledge the Ministry of Science and Technology, Taiwan, for financial support under Grant MOST 104-2218-E-002-006.

References

[1] Heisler EG, Hunter AS, Siciliano J, Treadway RH. Solute and temperature effects in the pervaporation of aqueous alcoholic solutions. Science 1956;124:77–9.
[2] Kudasheva A, Sorribas S, Zornoza B, Téllez C, Coronas J. Pervaporation of water/ethanol mixtures through polyimide based mixed matrix membranes containing ZIF-8, ordered mesoporous silica and ZIF-8-silica core-shell spheres. J Chem Technol Biotechnol 2015;90:669–77.
[3] Feng X, Huang RYM. Liquid separation by membrane pervaporation: a review. Ind Eng Chem Res 1997;36:1048–66.
[4] Kita H, Sasaki S, Tanaka K, Okamoto K-i, Yamamoto M. Esterification of carboxylic acid with ethanol accompanied by pervaporation. Chem Lett 1988;17:2025–8.
[5] Bagnell L, Cavell K, Hodges AM, Mau AWH, Seen AJ. The use of catalytically active pervaporation membranes in esterification reactions to simultaneously increase product yield, membrane permselectivity and flux. J Membr Sci 1993;85:291–9.
[6] Lv B, Liu G, Dong X, Wei W, Jin W. Novel reactive distillation–pervaporation coupled process for ethyl acetate production with water removal from reboiler and acetic acid recycle. Ind Eng Chem Res 2012;51:8079–86.
[7] Kouzu M, Nakagaito A, Hidaka J-s. Pre-esterification of FFA in plant oil transesterified into biodiesel with the help of solid acid catalysis of sulfonated cation-exchange resin. Appl Catal A 2011;405:36–44.
[8] Ghazali M, Nawawi M, Huang RYM. Pervaporation dehydration of isopropanol with chitosan membranes. J Membr Sci 1997;124:53–62.
[9] Wu KCW, Kang C-H, Lin Y-F, Tung K-L, Deng Y-H, Ahamad T, et al. Towards acid-tolerated ethanol dehydration: chitosan-based mixed matrix membranes containing cyano-bridged coordination polymer nanoparticles. J Nanosci Nanotechnol 2016;16:4141–6.
[10] Lee K-R, Teng M-Y, Hsu T-N, Lai J-Y. A study on pervaporation of aqueous ethanol solution by modified polyurethane membrane. J Membr Sci 1999;162:173–80.
[11] Liu Y-L, Hsu C-Y, Su Y-H, Lai J-Y. Chitosan−silica complex membranes from sulfonic acid functionalized silica nanoparticles for pervaporation dehydration of ethanol−water solutions. Biomacromolecules 2005;6:368–73.
[12] Elnahrawy AM, Kim YS, Ali AI. Synthesis of hybrid chitosan/calcium aluminosilicate using a sol-gel method for optical applications. J Alloys Compd 2016;676:432–9.
[13] Yang D, Li J, Jiang Z, Lu L, Chen X. Chitosan/TiO2 nanocomposite pervaporation membranes for ethanol dehydration. Chem Eng Sci 2009;64:3130–7.
[14] Gerard N, Santhana Krishnan R, Ponnusamy SK, Cabana H, Vaidyanathan VK. Adsorptive potential of dispersible chitosan coated iron-oxide nanocomposites toward the elimination of arsenic from aqueous solution. Process Saf Environ Prot 2016;104, A:185–95.
[15] Dudek G, Gnus M, Strzelewicz A, Turczyn R, Krasowska M. Permeation of ethanol and water vapors through chitosan membranes with ferroferric oxide particles cross-linked by glutaraldehyde and sulfuric(VI) acid. Sep Sci Technol 2016;51:2649–56.
[16] Xing R, Wu H, Zhao C, Gomaa H, Zhao J, Pan F, et al. Fabrication of chitosan membranes with high flux by magnetic alignment of in situ generated Fe_3O_4. Chem Eng Technol 2016;39:969–78.
[17] Djerahov L, Vasileva P, Karadjova I, Kurakalva RM, Aradhi KK. Chitosan film loaded with silver nanoparticles—sorbent for solid phase extraction of Al(III), Cd(II), Cu(II), Co(II), Fe(III), Ni(II), Pb(II) and Zn(II). Carbohydr Polym 2016;147:45–52.
[18] Kamal MA, Bibi S, Bokhari SW, Siddique AH, Yasin T. Synthesis and adsorptive characteristics of novel chitosan/graphene oxide nanocomposite for dye uptake. React Funct Polym 2017;110:21–9.
[19] Zhang L, Luo H, Liu P, Fang W, Geng J. A novel modified graphene oxide/chitosan composite used as an adsorbent for Cr(VI) in aqueous solutions. Int J Biol Macromol 2016;87:586–96.
[20] Fan L, Luo C, Li X, Lu F, Qiu H, Sun M. Fabrication of novel magnetic chitosan grafted with graphene oxide to enhance adsorption properties for methyl blue. J Hazard Mater 2012;215–216:272–9.
[21] Han D, Yan L, Chen W, Li W. Preparation of chitosan/graphene oxide composite film with enhanced mechanical strength in the wet state. Carbohydr Polym 2011;83:653–8.
[22] Fan L, Luo C, Sun M, Li X, Lu F, Qiu H. Preparation of novel magnetic chitosan/graphene oxide composite as effective adsorbents toward methylene blue. Bioresour Technol 2012;114:703–6.
[23] Liu Y-H, Liu Q-S, Zhang Z-H. Amberlyst-15 as a new and reusable catalyst for regioselective ring-opening reactions of epoxides to β-alkoxy alcohols. J Mol Catal A 2008;296:42–6.
[24] Peters TA, Benes NE, Holmen A, Keurentjes JTF. Comparison of commercial solid acid catalysts for the esterification of acetic acid with butanol. Appl Catal A 2006;297:182–8.
[25] Tung K-L, Chang K-S, Wu T-T, Lin N-J, Lee K-R, Lai J-Y. Recent advances in the characterization of membrane morphology. Curr Opin Chem Eng 2014;4:121–7.
[26] S. Stankovich, D.A. Dikin, R.D. Piner, K.A. Kohlhaas, A. Kleinhammes, Y. Jia, et al., Synthesis of graphene-based nanosheets via chemical reduction of exfoliated graphite oxide, Carbon 2007; 45: 1558–65.
[27] Williams G, Seger B, Kamat PV. TiO2-graphene nanocomposites. UV-assisted photocatalytic reduction of graphene oxide. ACS Nano 2008;2:1487–91.
[28] Dreyer DR, Park S, Bielawski CW, Ruoff RS. The chemistry of graphene oxide. Chem Soc Rev 2010;39:228–40.
[29] Pawlak A, Mucha M. Thermogravimetric and FTIR studies of chitosan blends. Thermochim Acta 2003;396:153–66.
[30] Buraidah MH, Arof AK. Characterization of chitosan/PVA blended electrolyte doped with NH4I. J Non-Cryst Solids 2011;357:3261–6.
[31] Marcano DC, Kosynkin DV, Berlin JM, Sinitskii A, Sun Z, Slesarev A, et al. Improved synthesis of graphene oxide. ACS Nano 2010;4:4806–14.
[32] Si Y, Samulski ET. Synthesis of water soluble graphene. Nano Lett 2008;8:1679–82.
[33] Rana VK, Choi M-C, Kong J-Y, Kim GY, Kim MJ, Kim S-H, et al. Synthesis and drug-delivery behavior of chitosan-functionalized graphene oxide hybrid nanosheets. Macromol Mater Eng 2011;296:131–40.
[34] Zuo P-P, Feng H-F, Xu Z-Z, Zhang L-F, Zhang Y-L, Xia W, et al. Fabrication of biocompatible and mechanically reinforced graphene oxide-chitosan nanocomposite films. Chem Cent J 2013;7 39-39.
[35] Coronas J, Santamaría J. Separations using zeolite membranes. Sep Purif Rev 1999;28:127–77.